Supplementary Information

Scalable fabrication of gap-plasmon-based dynamic and chromogenic nanostructures by capillary-interaction driven self-assembly of liquid-metal

Renu Raman Sahu, Alwar Samy Ramasamy, Santosh Bhonsle S, Mark Vailshery D C, Tapajyoti Das Gupta*

Laboratory of Advanced Nanostructures for Photonics and Electronics, Department of Instrumentation and Applied Physics, Indian Institute of Science, C. V. Raman Road, Bengaluru-560012, India

E-mail: tapajyoti@iisc.ac.in

13 TABLE OF CONTENTS

43

1. Methods

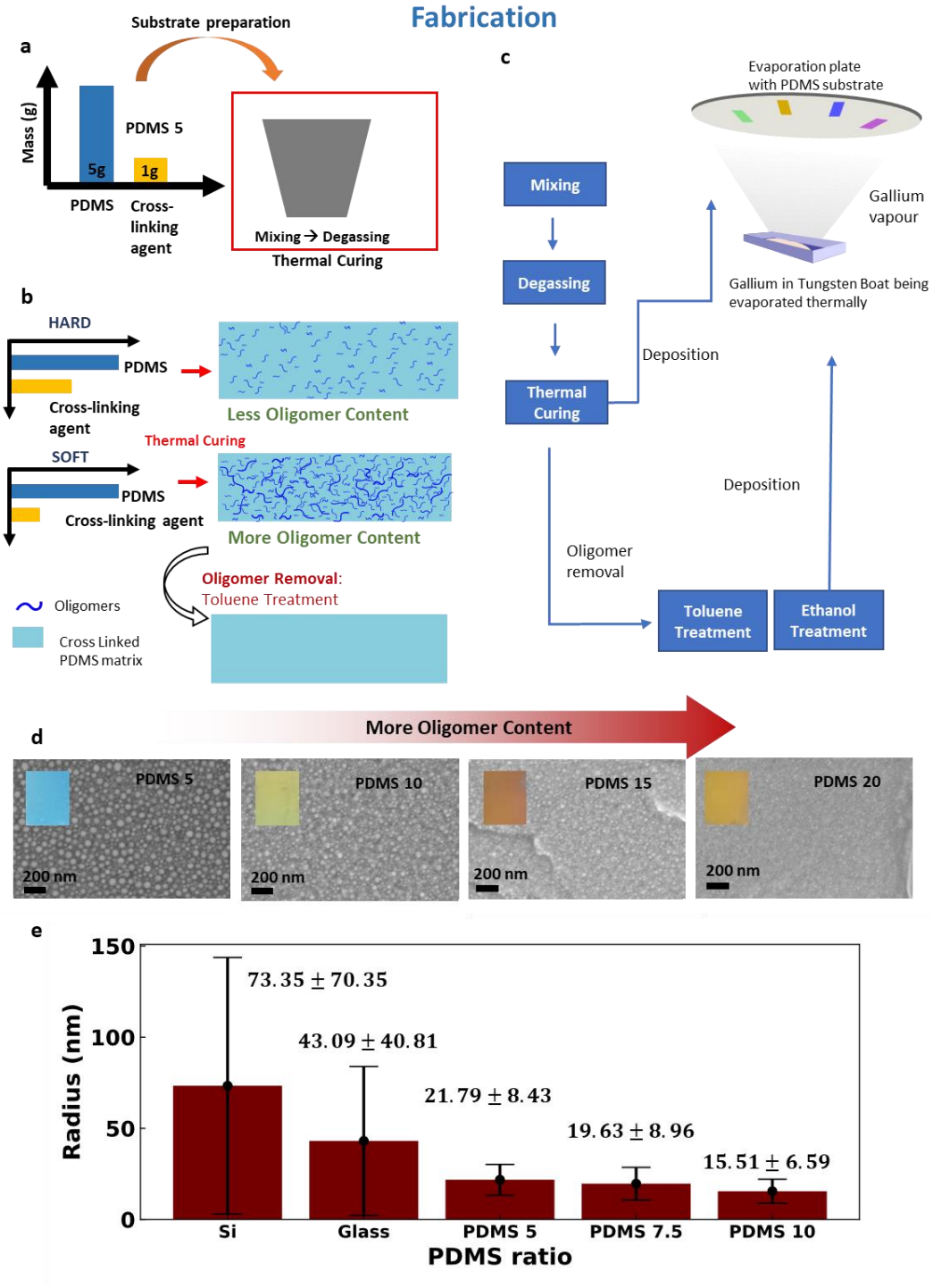

Figure 1: a, Schematic of Fabrication of different PDMS ratios. b, Schematic diagram of the PDMS substrates fabricated with different ratios of PDMS base and curing agent, and the effect of Toluene treatment on the PDMS substrate. c, Thermal evaporation of Gallium. d, The top view SEM images of PDMS ratios 5, 10, 15, 20 (from left to right). The optical images of Ga deposited on the substrates are shown in the inset. e, Average and standard deviation of radii of Ga nanodroplets formed on the substrates Si, Glass, PDMS 5, 7.5 and 10 after thermal evaporation.

1.1 Preparation of PDMS

Polydimethylsiloxane (PDMS) soft substrates are prepared by mixing the liquid PDMS base and curing agent in various ratios (Dow Corning, Sylgard 184). The following notation PDMS XX represents 1 part of curing agent is added to XX parts of liquid PDMS base in weight ratio. Substrate softness increases with an increase in the proportion of liquid PDMS base. To fabricate the structural color from Ga, PDMS 5, PDMS 10, PDMS 15, and PDMS 20 are chosen as substrates. The mixture is stirred thoroughly and desiccated to remove the bubbles. The solution is poured onto a Polystyrene (PS) petri-dish and cured at 80°C in an oven for 2 hours to attain a cured soft substrate, which inherently has some uncrosslinked liquid PDMS chains. Liquid Gallium is then thermally evaporated (HHV thermal evaporator) and deposited onto these substrates to form nanodroplets. The thickness and temperature of the substrates are monitored via inbuilt thickness and temperature monitoring sensors, respectively.

1.2 Toluene Treatment of PDMS substrates

To examine the role of uncrosslinked liquid PDMS chains, cured PDMS substrates are stirred in a toluene bath for a specific duration of time. This process dissolves the uncrosslinked liquid PDMS chains since toluene acts as a suitable solvent. During this period, toluene is changed in an interval of 24 hours. Subsequently, the PDMS substrate is immersed in ethanol for 12 hours and kept in a vacuum oven at 70°C for 12 hours to remove the solvent in the sample.

1.3 Elastic Modulus of PDMS substrates: with and without Oligomers

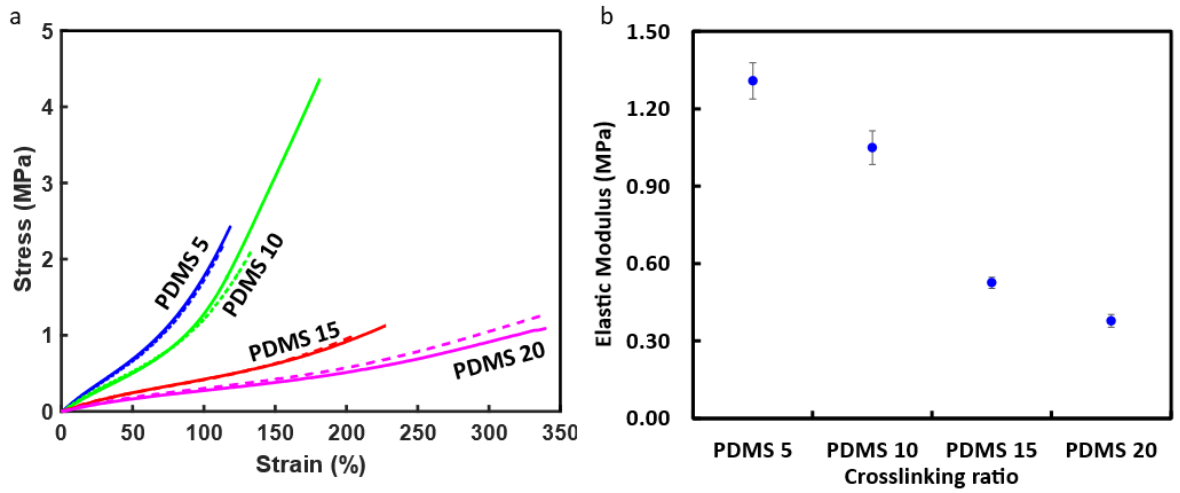

Figure 2: a, Stress-Strain plots of different PDMS samples with oligomers (solid line) and without oligomers (dotted line) subjected to a tensile strain in the Universal Testing Machine (UTM). b, Elastic modulus of different PDMS crosslinked substrates measured from the stress-strain curve with upto 40% strain, where the stress and strain are linear.

1.4 Effect of liquid oligomers of PDMS on the Gallium nanostructures

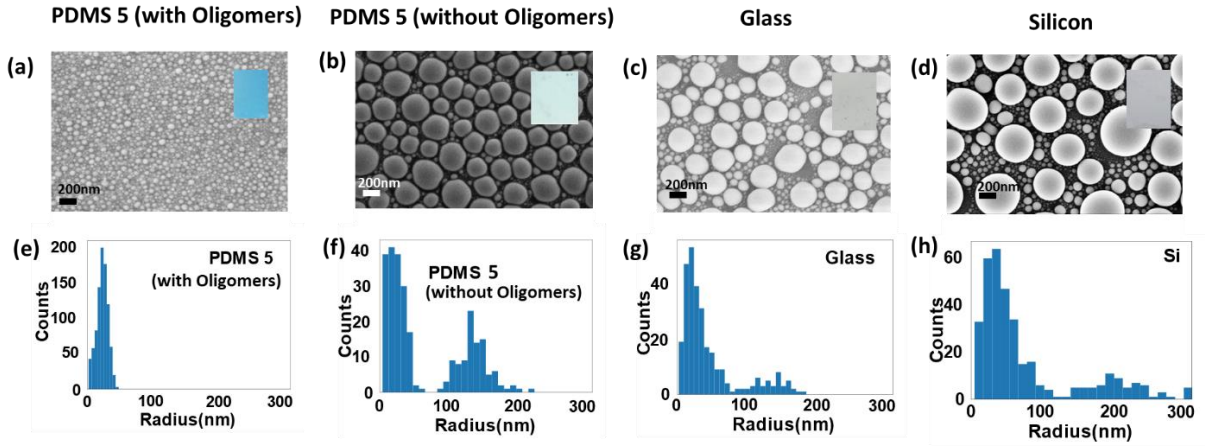

Figure 3: Top view SEM images when Ga is deposited onto (a) PDMS (with oligomers), (b) PDMS 5, (without oligomers), (c) Glass and (d) Silicon. The size distribution of Ga nanodroplets formed on the substrates (e) PDMS 5 (with oligomers), (f) PDMS 5, (without oligomers), (g) Glass and (h) Silicon.

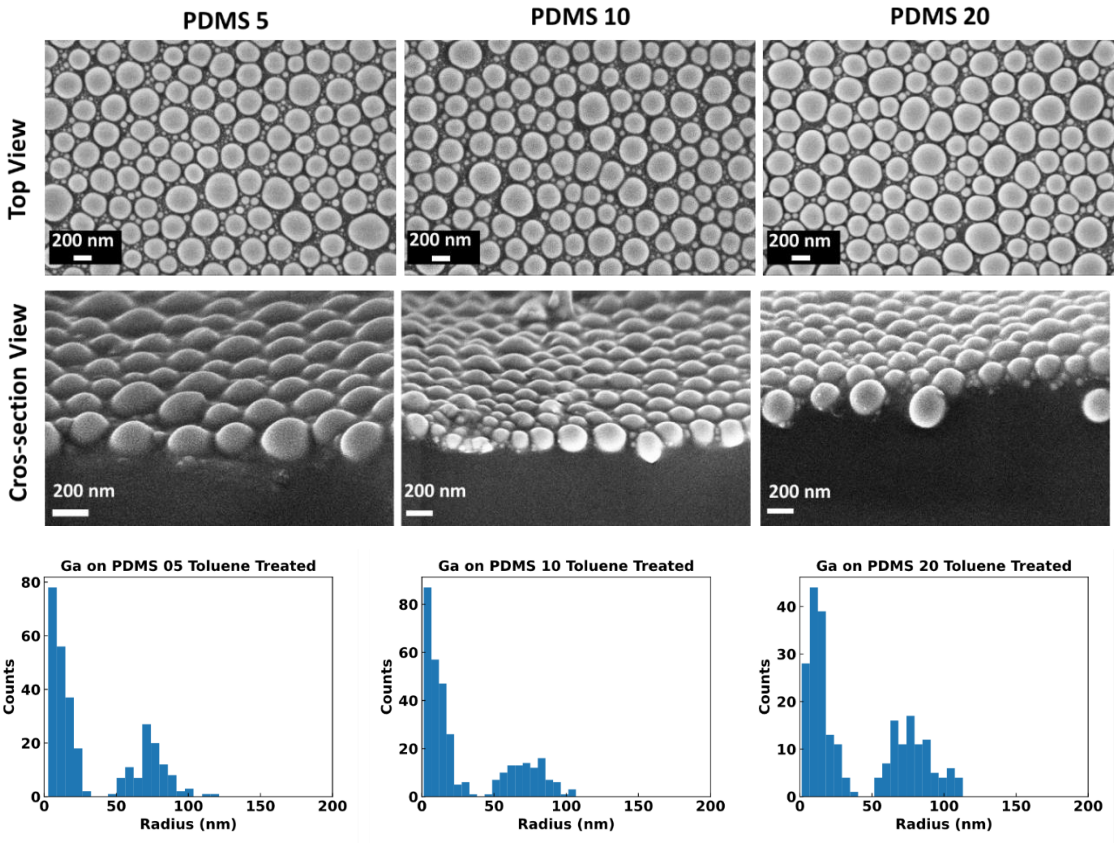

Figure 4: Top-view (top panel) and cross-sectional (middle panel) SEM images of Ga nanostructures on PDMS 5, 10, and 20 after removal of oligomers by toluene treatment and their corresponding size distribution is shown in the bottom panel.

The size distribution of Ga nanoparticles on PDMS substrates without oligomers is similar, characterized by large droplets of radii varying between 50 and 100 nm, and small droplets with radii less than 50 nm. Although Young's modulus of the substrates varies (SI Figure 2), the absence of

liquid oligomer content eliminates the difference in the size distribution of the Ga nanodroplets. This establishes that the fluidic interaction between the liquid oligomers and liquid Ga droplet results in a layered nanodroplets structure, thus producing colors.

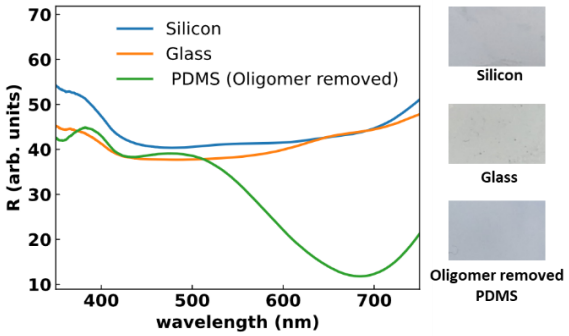

Figure 5: Reflectivity spectra of Ga deposited Si, Glass and Toluene treated PDMS. (Right column) Optical images of Ga deposited simultaneously on Si, glass and PDMS substrates without oligomers (Toluene treated).

Thus, we conclude that removing oligomers eliminates the distinction between different PDMS ratios. Therefore, oligomers play a crucially significant role in the determination of nanostructures.

2. Mathematical modeling of Ga nanostructure formation on PDMS: Substrate, Growth and Engulfing Equations

In this section, we hypothesize the formation mechanism of Ga nanospheres and their embedding into the PDMS. Also, we propose a set of differential equations based on a few assumptions to model the experimentally observed size distribution trends of Ga nanodroplets.

2.1 Nucleation and formation of droplets of critical radii

Thermal evaporation of Gallium onto the substrate results in Ga vapors near the PDMS substrate, which condenses to form nanospheres. The surface tension of Ga renders the droplets to be spheres. The formation of a Liquid Ga-air interface costs energy proportional to the surface area of the sphere, whereas condensation into liquid droplets releases its vaporisation energy proportionate to its volume. Therefore there would be a critical radius which would be the minimum radius of Ga nanodroplets that form upon condensation. Once the Ga nanodroplets form, they grow due to further condensation of Ga vapor to the liquid droplet of a few nanometers radius before it comes into contact with the PDMS substrate.

2.2 Initial deformation of the substrate due to Laplace pressure

When the nanodroplets come in contact with the substrate, the initial speed it and its Laplace pressure will result in the substrate's initial deformation, leading to a small immersion of the nanodroplet into PDMS. Once infinitesimal immersion happens, the contact line of Ga droplet and PDMS occurs, and the following sequence of events occur.

Young's law governs the wetting of droplets on rigid substrates and Neumann's triangle on liquid substrates, which is infinitely soft[1]. In between the rigid and liquid substrates called the soft solids, the contact angle for larger droplets follows Young's law, whereas, with the smaller droplets, the contact angle is obtained by the balance of Neumann's triangle. In soft solids, the balance between capillarity and elastic forces is governed by the elastocapillary length scale $l_{el} = \frac{\gamma_{Ga}}{E}$, where γ_{Ga} is the surface tension of the gallium droplet, and E is Young's modulus. For the magnitude of radius $R > l_{el}$, ridge formation at the contact line is small, and macroscopically droplets follow Young's law like a rigid substrate. Whereas for small droplets $R < l_{el}$, high Laplace pressure inside the droplet can deform and form a dimple on the substrate. In such cases, the droplet profile takes the shape of a liquid lens which is given by the balance of γ_{Ga}, Υ_{PDMS} and $\Upsilon_{PDMS-Ga}$. The elastocapillary length for a Ga droplet on PDMS 5 is 496. During typical evaporation, the radius of the Ga droplet is observed to be around 25 nm. Hence the droplet will resemble the case of a liquid lens on PDMS substrates.

2.3 Assumption of spherical geometry of partially immersed Gallium nanodroplets

The Ga droplet on PDMS can be considered to be placed equivalently on a liquid substrate from the elastocapillary length scale analysis (Sec 2.2). As a result, the shape of a Ga droplet on a PDMS substrate is governed by the balance of interfacial stresses (surface tension forces) at the three-phase contact line, which is well characterized by Neumann's triangle[2]. The balance of forces in horizontal and vertical directions gives,

$$\gamma_{Ga}\cos\alpha + \gamma_{Ga-PDMS}\cos\beta - \gamma_{PDMS}\cos\sigma = 0 \qquad (1)$$

$$\gamma_{Ga}\sin\alpha - \gamma_{Ga-PDMS}\sin\beta + \gamma_{PDMS}\sin\sigma = 0 \qquad (2)$$

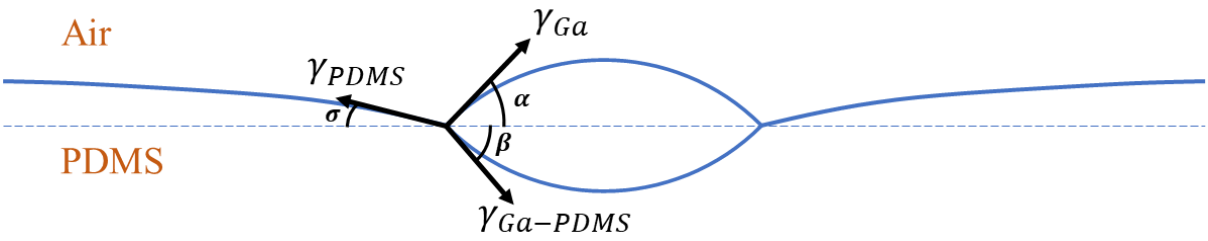

142

143 *Figure 6: Schematic of Ga droplet on PDMS substrate for very high elastocapillary length compared to the droplet radius.*

144 From the cosine law of the triangle, relation between the angle made by the different liquid with
145 horizontal and surface energies can be expressed as,

$$\alpha + \beta = \cos^{-1}\frac{\gamma_{PDMS}^2 - \gamma_{Ga-PDMS}^2 - \gamma_{Ga}^2}{2\gamma_{Ga}\gamma_{Ga-PDMS}} \quad (3)$$

$$\alpha + \sigma = \pi - \cos^{-1}\frac{\gamma_{Ga-PDMS}^2 - \gamma_{Ga}^2 - \gamma_{PDMS}^2}{2\gamma_{Ga}\gamma_{PDMS}} \quad (4)$$

146

147 From the geometrical analysis, the volume occupied by Ga with the Gallium-air and PDMS-Gallium
148 interfaces can be calculated as,

$$V_1 = \frac{\pi R_d^3}{3\sin^3\alpha}(1-\cos\alpha)^2(2+\cos\alpha) \quad (5)$$

$$V_2 = \frac{\pi R_d^3}{3\sin^3\beta}(1-\cos\beta)^2(2+\cos\beta) \quad (6)$$

149

150 Equating the volume in the Ga of occupied with two different arcs of radius to the volume of the
151 initial spherical droplet $V_1 + V_2 = V$, contact radius R_d can be found. With the contact radius, radius
152 of the lens formed by the Ga droplet can be determined by,

$$R_1 = \frac{R_d}{\sin\alpha} \quad (7)$$

$$R_2 = \frac{R_d}{\sin\beta} \quad (8)$$

153

154 Since the surface energies of Ga-air and Ga-PDMS interface are close, the exposed and immersed
155 radius of curvature is almost the same. For example, for a Ga droplet of 200 nm diameter, the exposed
156 and immersed radii are 102.4nm and 100nm. This enables us to assume a spherical geometry of Ga
157 nanodroplet even during immersion into the PDMS.

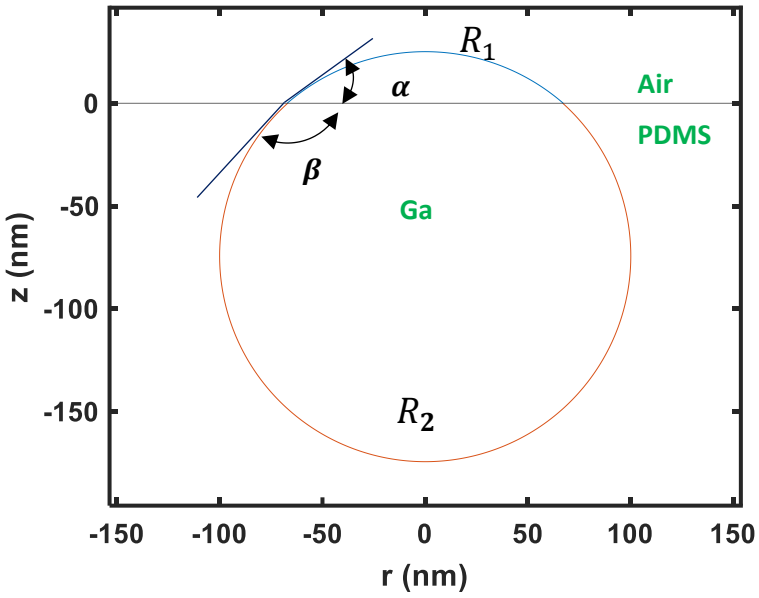

Figure 7: The shape of the Ga droplet (200 nm diameter) on the PDMS substrate is calculated analytically. Gravity is neglected at the nanoscale, leading to equal pressure across both air and PDMS phases and hence the curve remains a flat line between both phases. From Neumann equilibrium conditions, contact angles are obtained, $\alpha = 40.8°$ and $\beta = 138°$. Using the angles and volume conservation, the radius of the spherical arcs are $R_1 = 102.4\ nm$ and $R_2 = 100\ nm$.

2.4 Positive spreading Parameter: Engulfing of Ga droplets layer

The phenomena of fluid separation and ridge formation occur when materials with a positive spreading parameter (defined in the manuscript) are used to swell PDMS[3,4]. The spreading parameter determines the minimum energy configuration of three interfaces. For our case, the spreading parameter S turns out to be

$$S = \gamma_{Ga-air} - \gamma_{Ga-oligomers} - \gamma_{oligomers-air} = 650 - 590 - 20 = 40\ mN/m \quad (9)$$

Here γ_{Ga-air}, $\gamma_{Ga-oligomers}$ and $\gamma_{oligomers-air}$ denote the surface tensions between Ga and air, Ga and oligomers, and oligomers and air. A positive spreading parameter of 40mN/m implies that the surface energies of Ga-air interface is 40 milliJoule per square meter more energy than that of the two interfaces Ga-oligomers and oligomers-air, combined. To minimize the surface energy of the system (for a positive spreading parameter), the oligomers will separate from the PDMS network and cloak the Ga nanodroplets. The mechanism of Gallium nanodroplets penetrating the PDMS is hypothesized here using the result for positive spreading parameter and a few assumptions made about the substrate and its interaction with Ga nanodroplets. The positive spreading coefficient ($S > 0$) of the system results in the extraction of oligomers from the cross-linked PDMS network and tends to cloak the nanodroplet. During engulfing, the nanodroplet pulls the oligomers to cloak it up. The surface undulations of the oligomers are energetically unfavorable as compared to a planar surface. Therefore, the surface tends to be planar, thus extracting more oligomers out of the cross-linked PDMS network. Moreover, the initial velocity of the nanodroplet into the PDMS contributes to their immersion.

2.5 Hypothesis of engulfing mechanism and Substrate-Growth-Engulfing (SGE) equations

Engulfing of the Ga nanodroplet is an interplay of the following three events co-occurring.

a) Separation of Oligomers from the PDMS network

Let f be the volume of liquid oligomers present in a given substrate volume in units of nm^3. The rate at which f changes when a Ga droplet-oligomer interaction takes place dictates the phenomena of oligomer separation and will be described by the expression $\frac{df}{dt}$.

b) Growth of Ga droplet

The rate of increase of radius R (in units of nm) Ga nanosphere describes its growth and is depicted by the expression $\frac{dR}{dt}$.

c) Engulfing of Ga nanodroplet

We define the engulfing angle θ (radian) as the polar angle of the contact line Ga-air-PDMS interface if one assumes the center of the sphere to be the origin and positive z-axis as the normal of undeformed PDMS-air interface from PDMS to air (SI Figure. 8). The rate $\frac{d\theta}{dt}$ describes the engulfing of Ga-droplet.

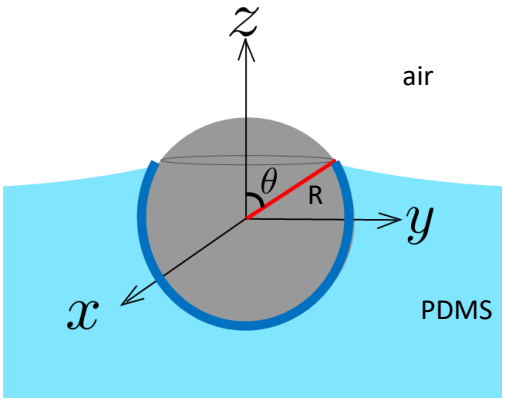

Figure 8: A partially immersed and engulfed Ga nanodroplet with an engulfing angle θ. Note that the exposed surface area is $S = 2\pi R^2(1 - cos\,\theta)$ and that immersed is $2\pi R^2(1 + cos\,\theta)$. When $\theta = 0$, it is the case of complete immersion. A completely immersed nanodroplet cannot grow, and hence the rate of change of radius vanishes. No,te that $S = 0$ at $\theta = 0$, indicating complete immersion. At $\theta = \pi, S = 4\pi R^2$, the entire surface is exposed and hence the rate of increase of radius is maximum.

In the following sections, we present the proposed model of these events in terms of differential equations. This set of differential equations describes the substrate-droplet interaction of a single nanodroplet.

2.6 Substrate Equation

Oligomers possess fluidic properties and are embedded homogeneously in the PDMS network. When a droplet touches the PDMS, the Ga-air-PDMS interface is formed and oligomers tend to diffuse from the bulk PDMS to the droplet interface and engulf it. This requires migration of the oligomers to the interface. Note that, at a given instant f is the total volume of oligomers present in the PDMS network available for migration towards interface and contribute to droplet-engulfing. The unit of f is that of volume (nm^3). The volume of oligomers used to engulf the nanodroplet will no longer be available in the PDMS network. We assume that a thin layer of thickness w nm of oligomers will engulf the nanodroplet in the

immersed area uniformly. We hypothesize that the rate at which f will deplete is proportional to the volume of oligomers left in the PDMS network after an engulfing of θ is,

$$\frac{df}{dt} \propto f - 2\pi R^2 w(1 + cos\,\theta)$$

The migration of oligomers toward the interface occurs due to the contact force and we assume it to be proportional to $2\pi R\ sin\,\theta$,

$$\frac{df}{dt} \propto 2\pi R\ sin\,\theta$$

With κ_s as the proportionality constant, we obtain

$$\frac{df}{dt} = -\kappa_s\big(f - 2\pi R^2 w(1 + cos\,\theta)\big)(2\pi R\ sin\,\theta) \qquad (10)$$

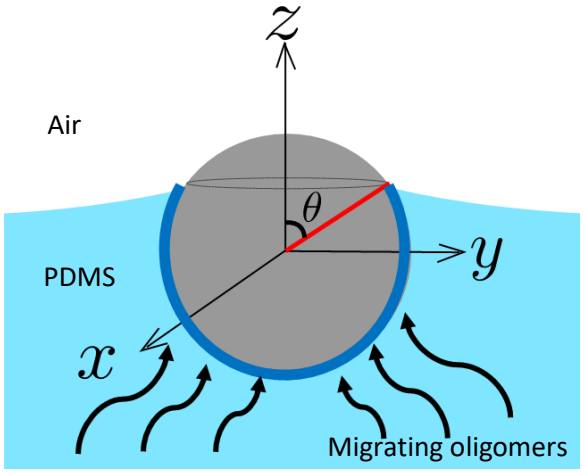

Figure 9: Schematic of oligomers migrating from the PDMS network to the interface of PDMS and Gallium. The Ga nanodroplet will be cloaked by a thin liquid oligomer layer.

Here κ_s is known as substrate constant and describes the ease of migration of oligomers through the PDMS network. It is a dimensional constant with units $nm^{-1}s^{-1}$. It does not vary during the process of engulfing because the cross-linked network is assumed not to change during engulfing. The negative sign on the right-hand side signifies the reduction of oligomers as they are used up for engulfing.

Intuition dictates that higher PDMS ratios (those with a lower proportion of curing agent) have a more volumetric fraction of oligomers in a given substrate volume and hence will be characterized by higher values of f.

2.7 Growth equation

The conversion from vapor to liquid occurring at the exposed surface area results in a change in the volume of the nanodroplet. Let ρ be the density of liquid Gallium (5.9 g/cc), and J the flux of liquid Ga entering the droplet through condensation. We can therefore write,

$$\rho \frac{d}{dt}\left(\frac{4}{3}\pi R^3\right) = 2\pi R^2(1 - cos\,\theta)J \quad (11)$$

or,

$$\frac{dR}{dt} = \frac{J}{2\rho}(1 - cos\,\theta) \quad (12)$$

or,

$$\frac{dR}{dt} = \kappa_\rho(1 - cos\,\theta) \quad (13)$$

Here $\kappa_\rho = \frac{J}{2\rho}$ is the growth constant with unit $nm\ s^{-1}$.

The growth constant is determined by the flux of Ga atoms condensing into the droplet, which depends on temperature and the density of Ga atoms in the vapor phase. One can experimentally control the number density of Ga atoms in vapor phase by manipulating the deposition rate during thermal evaporation. More is the number density of Ga-atoms in the vapor phase, the faster the condensation into the liquid droplet phase.

Temperature plays a crucial role in determining the vapor-liquid equilibrium of Ga. A higher temperature favors the vapor phase, and hence the rate of condensation decreases, which causes a reduction in J and a lowering of the growth constant κ_ρ.

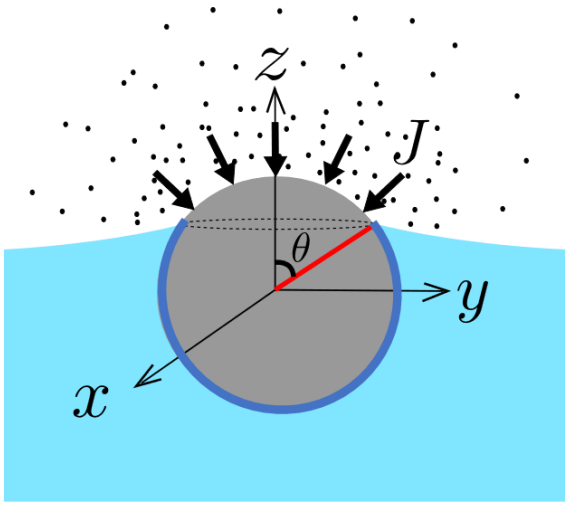

Figure 10: Schematic of the Ga vapor liquefying at the interface of Ga vapor and nanodroplet. The flux of Ga atoms condensing into the droplet is directly proportional to the number density around the exposed surface of the Ga droplet. With the increase in temperature, the probability of Ga atoms being in a vapor state increases, thus reducing the flux of condensing Ga atoms.

2.8 Engulfing Equation

The initial immersion due to the Laplace pressure of the Ga droplet renders the initial value of θ to be $\pi - h$, where $h \ll 1$. As the engulfing occurs, its value decreases towards $\theta = 0$, which is the case of complete engulfing.

We hypothesize that the rate at which engulfing occurs is proportional to the amount of oligomers available for migrating towards the interface and contributing to engulfing. Thus, we can write

$$\frac{d\theta}{dt} = -\kappa_e\left(f - 2\pi R^2 w(1 + cos\,\theta)\right) \quad (14)$$

where κ_e is the engulfing constant with unit $nm^{-3}s^{-1}$.

2.9 Iteration Procedure to obtain the number of immersed layers.

The substrate-growth-engulfing (SGE) equations describe the substrate droplet equation for a single droplet. The boundary conditions for the equations are defined by θ, from infinitesimal engulfing ($\theta = \pi - h$) to complete engulfing ($\theta = 0$). During this process, f decreases and the radius R of the nanodroplet increases. There are ample oligomers for engulfing the initial layers (the deepest layer observed in the SEM image). The rate of engulfing would be faster for the droplets in these layers; hence the growth time is relatively less than the droplets from the top layer. Here the engulfing phenomena dominate, and complete engulfing takes place. For the subsequent layers of droplets, the amount of oligomers is depleted, thus reducing the rate of engulfing and increasing the growth time. For the topmost layer, the growth time dominates the engulfing time and partial engulfing occurs.

To model the above picture, we solve the SGE equations for a nanosphere with an arbitrary but reasonable choice of initial radius and a thickness of oligomer coating around it. The initial volume of oligomers f is chosen reasonably as well. The values of SGE constants κ_s, κ_e and κ_ρ, decide complete or partial engulfing. If complete engulfing occurs, the initial value of f for the next layer will be the final value of f in the case of a most recent engulfed droplet. Once the partial engulfing occurs, we stop the iteration and infer the number of iterations required to obtain the partial engulfing, which is the number of layers of Ga nanodroplets formed in the PDMS.

2.10 Results from SGE equations

On imposing the condition that the immersion angle is monotonically non-increasing with time, solutions of the SGE differential equations for a single droplet determine whether complete immersion will occur. The value of R at $\theta = 0$ (complete engulfing) is the final radius of the droplet.

To demonstrate an example, let us consider a PDMS substrate parametrized by $f_0 = 3000\,nm^3$ and substrate constants $\kappa_s = 0.3nm^{-1}s^{-1}$, $\kappa_\rho = 500nm\,s^{-1}$ and $\kappa_e = 0.1\,nm^{-3}s^{-1}$. We choose the initial radius of the droplet $R_0 = 4nm$ and the thickness of liquid oligomers engulfing it to be $w = 1nm$. The choice of the initial infinitesimal engulfing is chosen to be $\theta = \pi - h$ with $h = 10^{-4}rad$. While solving the SGE equations numerically, we deliberately impose θ to be monotonically decreasing and non-negative. Boundary values that satisfy these conditions for θ result in physically acceptable solutions.

1st layer

The first iteration of the numerical solution of SGE equations results in the monotonic decrease of θ from infinitesimal engulfing ($\theta = \pi - h$) to complete engulfing ($\theta = 0$). During this time, the radius of the nanodroplet increases from 4nm to 9.9nm, and the volume of oligomers decreases from $f = 3000nm^3$ to $f = 2691nm^3$.

The radius of the Ga droplet for the first layer is 9.9nm. The remaining volume of oligomers, $f = 2691nm^3$ will be used as the initial oligomer volume f_0 for the next iteration.

:

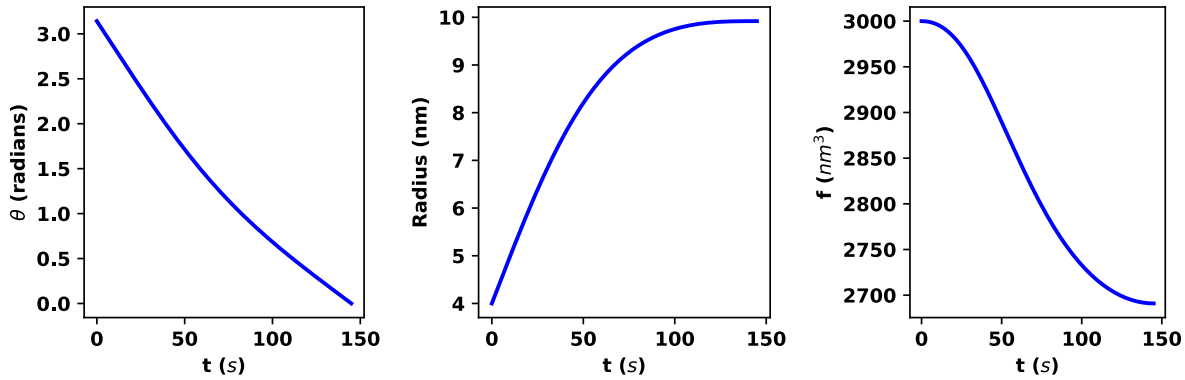

Figure 11: Graphs of (left) engulfing angle θ vs time t. (center) Radius (R) of Ga in the first layer vs. time t. (right) Volume of oligomers f vs. time t. These are the solutions of SGE equations for the first iteration. One can infer that complete engulfing occurs here, leading to the final radius of the Ga nanodroplet being 9.9nm.

2nd layer

The second iteration also results in complete engulfing, with a final Ga nanodroplet radius of 10.9 nm. Note that the radius is greater than that obtained in the previous layer. The remaining volume of oligomers $f = 2360nm^3$ is used as the initial oligomer volume for the next iteration.

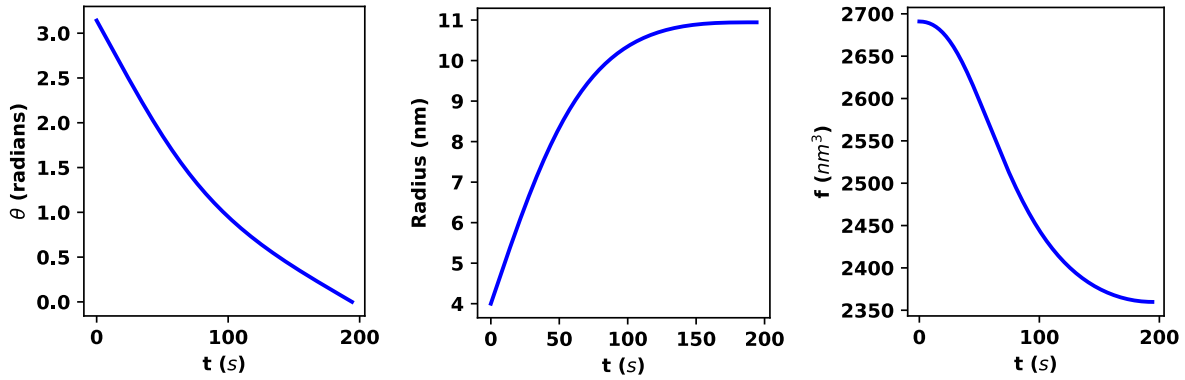

Figure 12: Graphs of (left) engulfing angle θ vs time t. (center) Radius (R) of Ga in the first layer vs. time t. (right) Volume of oligomers f vs. time t. These are the solutions of SGE equations for the second iteration. One can infer that complete engulfing occurs here, leading to the final radius of the Ga nanodroplet being 10.9nm.

3rd layer

In the third iteration, the final engulfing angle is $\theta = 0.6\,rad = 34^o$, thus indicating an incomplete immersion. This would be the topmost layer of the Ga droplets deposited onto the PDMS. The droplets at this layer have a radius of 13.3 nm, which is larger than the radius of droplets in the immersed layers.

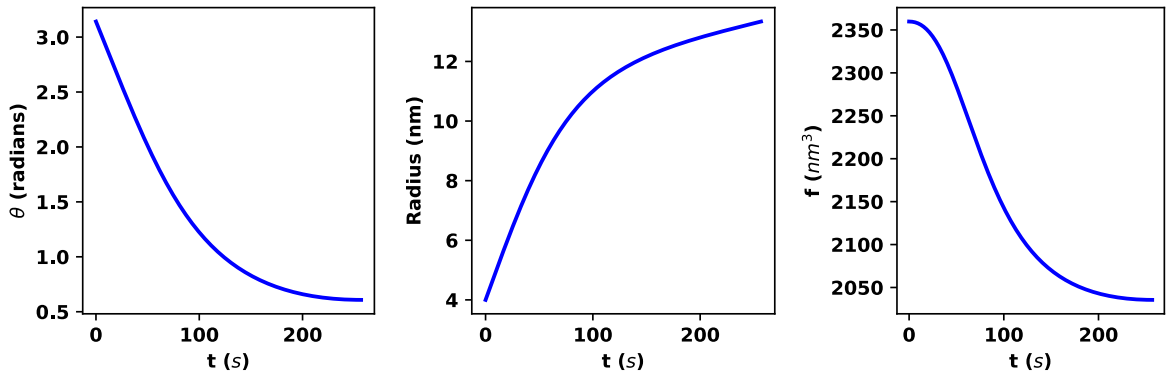

Figure 13: Graphs of (left) engulfing angle θ vs time t. (center) Radius (R) of Ga in the first layer vs. time t. (right) Volume of oligomers f vs. time t. These are the solutions of SGE equations for the third iteration. One can infer that incomplete engulfing occurs here. Hence it would be considered the topmost layer. The radius of the Ga particle formed here is 13.3 nm.

Thus, we obtain the depth profile of the Ga nanodroplet radius, as shown in the following figure.

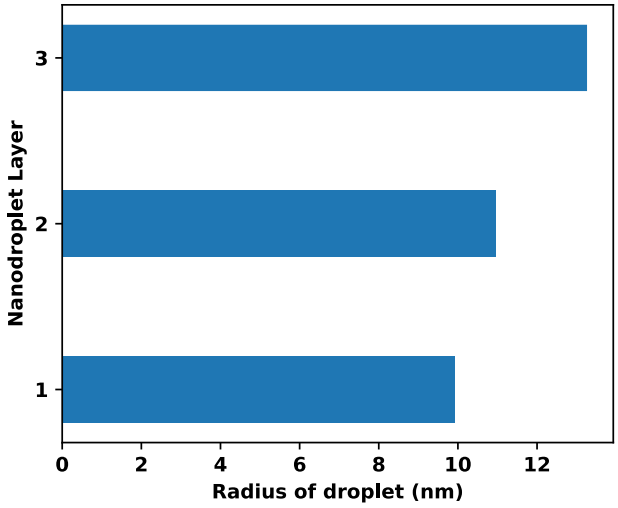

Figure 14: Histogram depicting the depth profile of Ga-radius across the cross-section. The deepest layer (1st layer) is the smallest in size. The size gradually increases with a decrease in depth. The topmost layer is of the highest radius. This trend matches with the observed cross-sectional images from SEM.

2.11 Comparison of the results from SGE equations with that from the experiments

As shown in the following figure, for each size distribution as observed in the cross-section images, there exist parameters of SGE equations which, when used to solve, give the matching results. The parameters used for the following three SEM images are tabulated as follows.

A note about the trend of parameters which gives the matching results for observed SEM images, are in order. The growth parameter $\kappa_\rho (= J/2\rho)$ is the same for all the PDMS substrates because the three samples were deposited simultaneously. The number density of Ga atoms in the vapor and the density of Ga are the same for all substrates during a particular

deposition. The initial radius is chosen arbitrarily but is the same for all three substrates because it is formed before the droplet encounters the substrates; hence it is independent of the substrate.

The substrate constant κ_s increases with the PDMS ratio. It measures the ease of movement of oligomers through the PDMS network. It is physically reasonable to argue that a higher PDMS ratio implies less cross-linking, making it easier for the oligomers to move through the PDMS network. More availability of oligomers means a faster engulfing, which explains the increasing trend of engulfing constant κ_e with PDMS ratio. The thickness of liquid oligomers encapsulating the nanodroplets is inferred to increase with the PDMS ratio from SGE equations. This can be consistently accommodated by the assumption that there is ample supply of the oligomers in higher PDMS ratios and hence a more increased thickness oligomer cloaking is favorable.

Parameters	PDMS 5	PDMS 10	PDMS 20
$\kappa_s(nm^{-1}s^{-1})$	0.4	0.5	0.8
$\kappa_\rho(nm\,s^{-1})$	1280	1280	1280
$\kappa_e\,(nm^{-3}s^{-1})$	0.1	0.11	0.15
$f_0(nm^3)$	4500	5000	7000
$R_0\,(nm)$	5.0	5.0	5.0
$w\,(nm)$	0.5	0.7	2.0

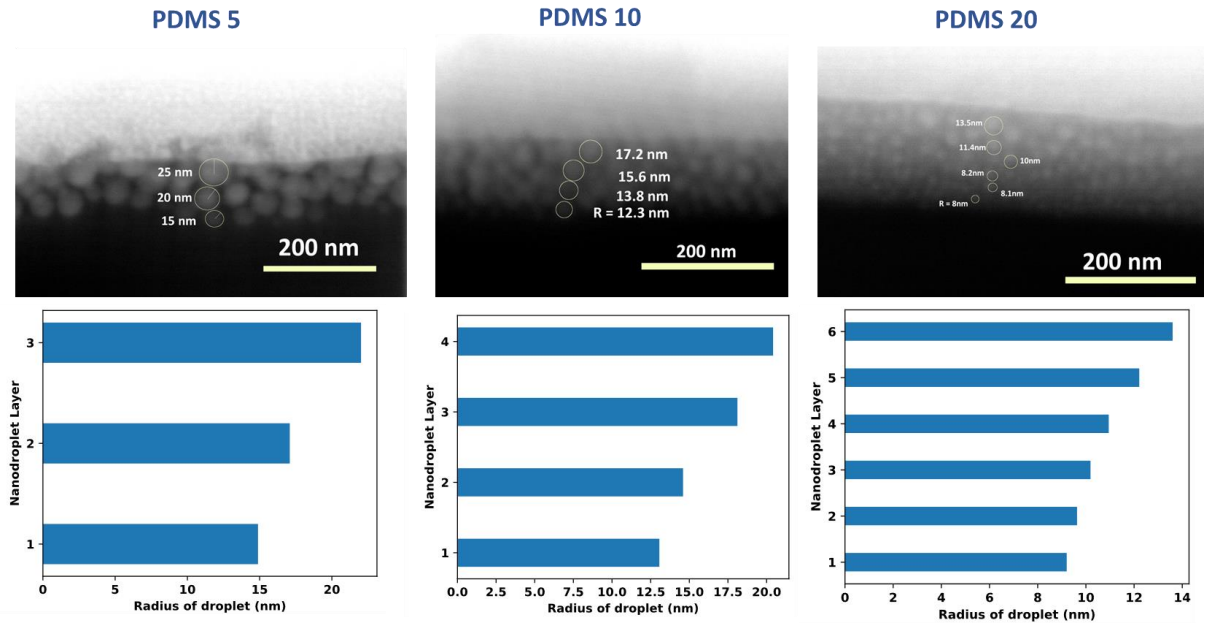

Figure 15: (Top) Table showing the parameters used for substrate-growth-engulfing (SGE) equations, matching the modeling results with the experiment's results. (Middle) The SEM images with representative circles are drawn around Ga nanodroplets to determine their radii. (Bottom) Results from SGE equations are solved using the parameters tabulated above. One can infer a fair agreement with the results from SGE equations and the observed SEM images.

2.12 Prediction from the SGE equation

The SGE equations have successfully explained the size distribution trends as observed experimentally. Once we have found the parameters for a particular deposition process and the PDMS substrates, we can use them and relate them with the experimental parameters to obtain a control on size distribution. For example, the rate of deposition and temperature will affect the growth constant κ_ρ. With the increase in the rate of deposition and decrease in temperature, κ_ρ increases. Though the exact analytical expression relating κ_ρ to these experimental parameters have not been determined yet, we can investigate the size distribution trend of varying them by changing the value of κ_ρ in SGE equations.

For example, consider PDMS 10, with SGE parameters obtained from SEM image analysis. The following figure depicts the effect of increasing the rate of deposition, which is effectively modeled by increasing the value of κ_ρ. We expect to obtain nanodroplets of larger sizes when we increase the deposition rate or lower the temperature. In the cross-section, the number of layers reduces.

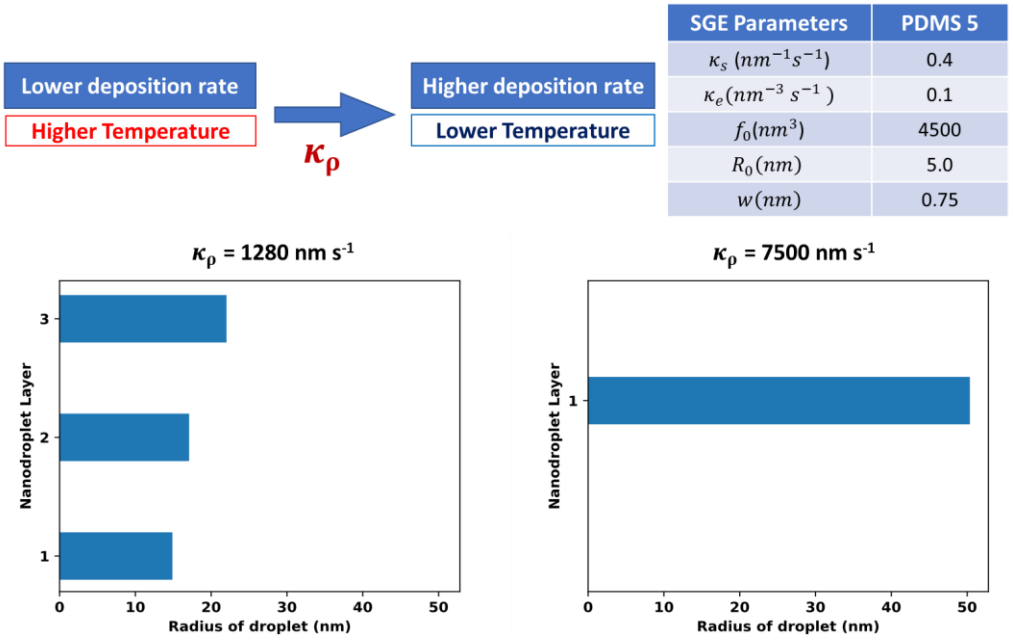

SGE Parameters	PDMS 5
$\kappa_s\ (nm^{-1}s^{-1})$	0.4
$\kappa_e(nm^{-3}\ s^{-1}\ )$	0.1
$f_0(nm^3)$	4500
$R_0(nm)$	5.0
$w(nm)$	0.75

Figure 16: The predicted trend of Ga-radius deposited on PDMS with varying rates of deposition or temperature. The table shows the parameters for PDMS 10 obtained from an SEM image of the sample deposited at the rate of 1Å/s (and $\kappa_\rho = 1280\ nm/s$, the leftmost SEM image). On increasing the deposition rate or lowering the temperature, we expect to get less number of Ga layers and nanodroplets of larger sizes.

Experimentally we observed that increasing the deposition rate to 7 Å/s from 1 Å/s decreased the number of layers of Ga nanodroplets. Moreover, the cross-sectional radius of Ga nanodroplets measured from the cross-section SEM image (see Figure 15) for lower rate deposition is 20.4±3.5 nm, while the higher rate of 7 Å/s is 49.9 ± 7.7 nm. This observation is in tandem with the predictions from SGE equations.

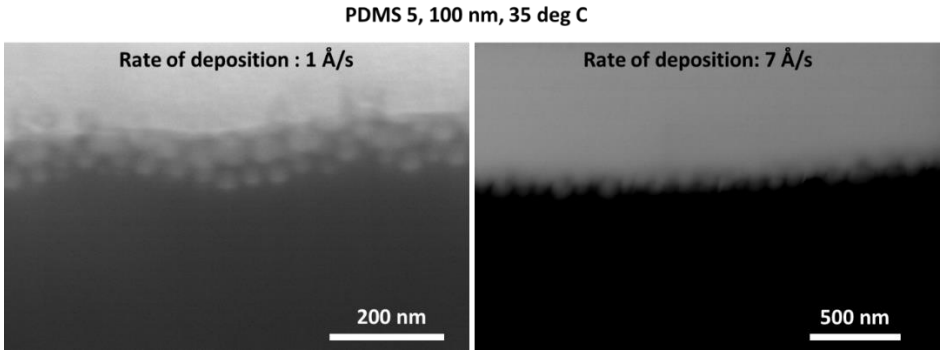

Figure 17: Cross-sectional Image of Ga deposited on PDMS 5 at 35 deg C with deposition rate (left) 1 Å/s, and (right) 7 Å/s.

The PDMS substrate is usually characterized by the ratio of the PDMS base to the cross-linking agent. The SGE equation provides another useful PDMS characterization utilizing SGE parameters. These parameters, as demonstrated in the previous section, describe substrate interaction with the gallium nanodroplets. It would be a novel method to describe the PDMS properties and their behavior with the Ga-deposition parameters.

3. Physics of Optical spectra of Ga deposited PDMS

By examining the reflectivity spectra of Ga-deposited PDMS, we can experimentally verify how light interacts with nanodroplets and gain insights into the morphology of Ga on PDMS. The results from SEM images confirm that the fluidic interaction of Gallium with the liquid oligomers of PDMS forms layers of Ga nanodroplets with varying radii. Due to encapsulation by oligomers, there will always be a dielectric Gap of refractive index 1.4 between the Ga nanodroplets. Its refractive index determines the optical properties of Ga. The real and imaginary parts of the refractive index of Ga are shown in the following figure[5].

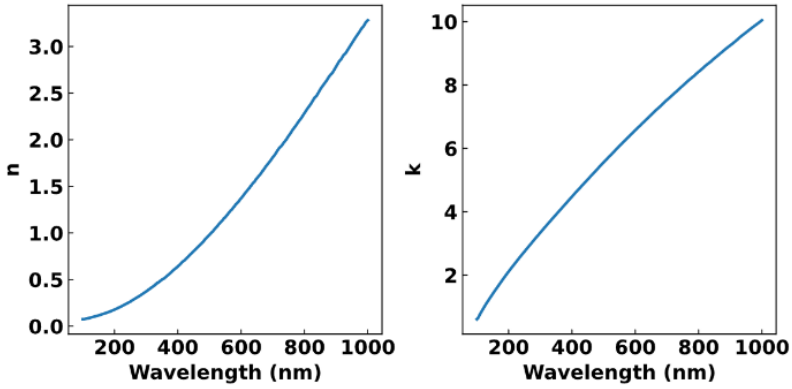

Figure 18: The real (left) and imaginary (right) part of the refractive index of Gallium.

Scanning electron microscopy shows that the structure of Ga nanodroplets on PDMS has the following structural characteristics:

1) The Gallium nanodroplets form several layers of nanodroplets, depending on the oligomer content of the PDMS. The more oligomer content more will be the number of layers.
2) The sizes of the Ga nanodroplets decrease with the depth of the Ga nanolayer into the PDMS.
3) An encapsulation of a thin layer of liquid oligomers separates each Ga nanodroplet.
4) For a given layer, the spatial location of Ga nanodroplets is random.

With the above constraints, we simulated some of the structures in Lumerical, a commercial FDTD software and observed a good match with the experimental reflectivity spectra.

FDTD was used with periodic boundary conditions along the x and y directions to simulate a large area of randomly distributed Ga nanostructures. The x-span and y-span were made large enough to cover a statistically significant number of Ga nanodroplets in each layer. Nevertheless, the periodicity would cause discrepancies between the experimentally obtained and the simulated reflectivity spectra. After achieving a satisfactory correlation between the experimental and simulated reflectivity spectra, the next step is comprehending the patterns observed in the reflectivity spectrum.

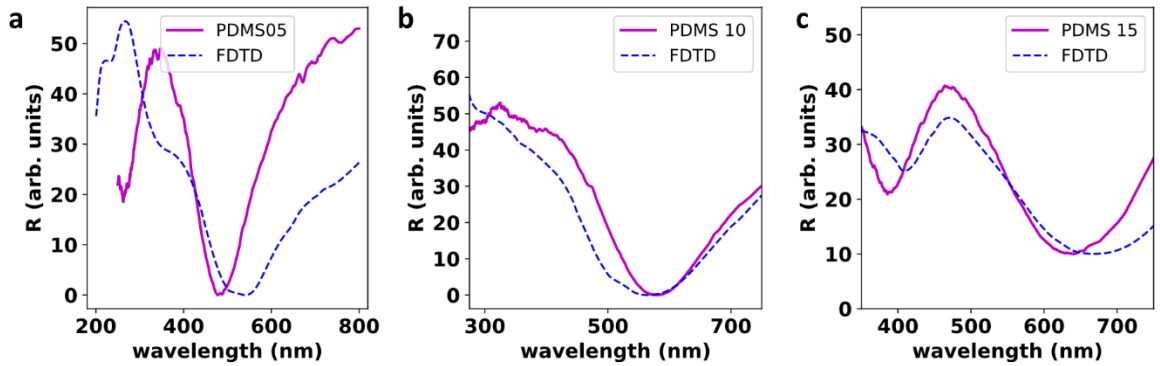

Figure 19: Lumerical simulation of FDTD region and the experimentally obtained reflectivity spectra of (a) PDMS 5, (b) PDMS 10 and (c) PDMS 15.

3.1 Variation of the spectrum with oligomer content

We observe that the spectral features of the reflectivity spectrum red-shift with an increase in the oligomer content (Figure 19). The observation is counter-intuitive given that higher oligomer content results in smaller particles; hence, one would expect a blue-shift. However, the electromagnetic fields in the inter-layer spatial region contribute to the spectrum, thus resulting in a red shift.

Although the sizes of Gallium nanodroplets decrease with the increase in the PDMS substrate's oligomer content, the spectral features consider the number and depth of the Ga nanodroplet layers. The structure with larger Ga nanodroplet layer depth results in red-shifted spectral features.

The intensity plots below depict the interaction of the incident electromagnetic field with different layers of Ga nanodroplets. At lower wavelengths, the electromagnetic field can interact with only the topmost layer of Ga spheres (see Figure 20g). In contrast, the higher wavelength fields can interact with all the layers of the structure (see Figure 20h and 20i).

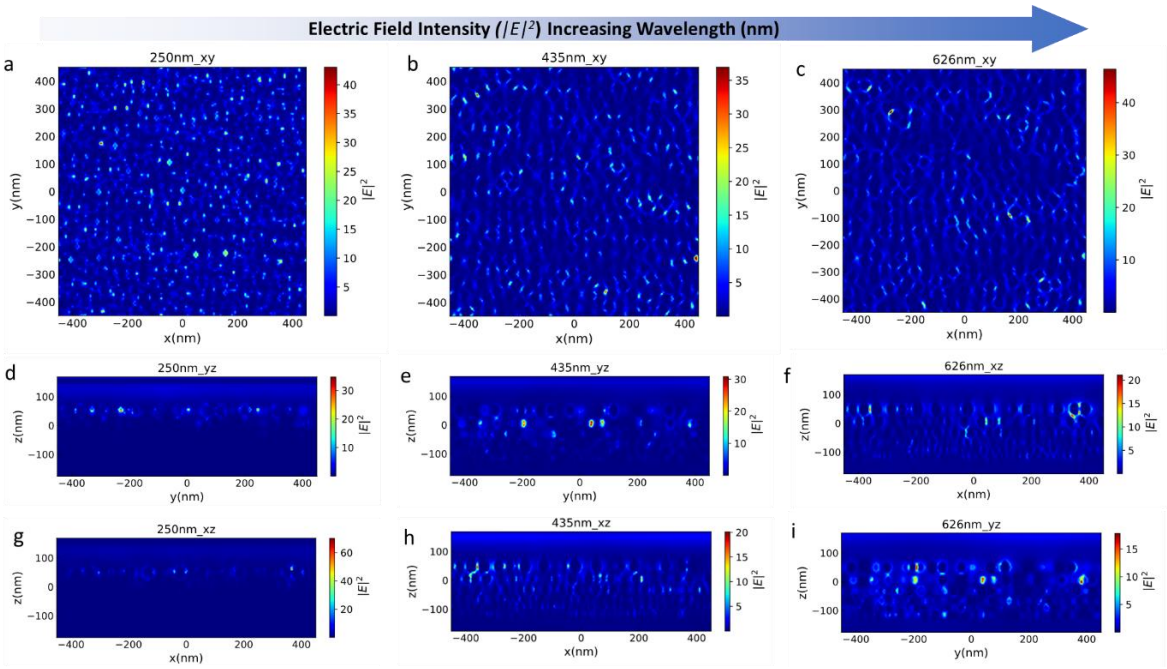

Figure 20: Electric field intensity plots at UV (250nm) and visible (435nm and 626nm) regions for the six-Layered structure of PDMS 15. (a-c) The Intensity plots in the XY plane of the first layer of Ga nanodroplets. (d-f) Field intensity at YZ plane. (g-i) Field intensity at XZ plane.

The following plot depicts the electric field intensity at some localized regions between two different layers of the Gallium nanodroplets. The incident electric field effectively sees a structure of feature size of the order of depth of the excited layers. Therefore the system in which the total thickness of Gallium droplet layers is larger will exhibit spectral features at larger wavelengths.

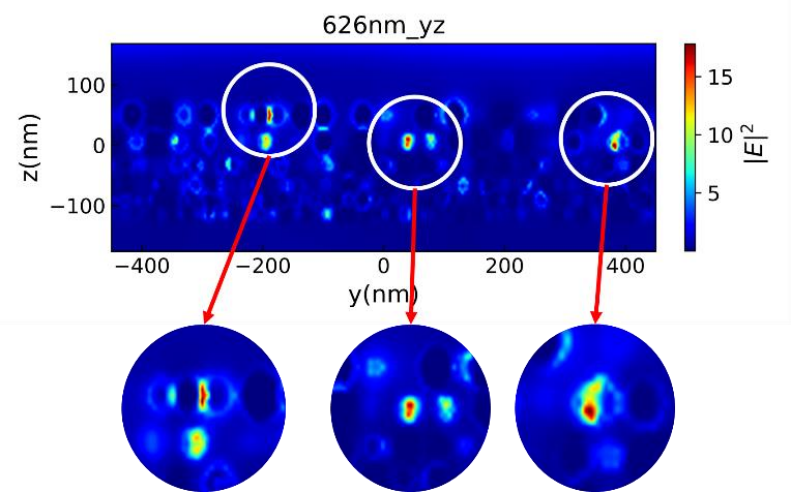

Figure 21: Electric field intensity plots at some localized regions between two different layers of the Gallium nanodroplets. The inter-layer field interaction causes the light to interact with the droplets in all the layers, thus equivalent to the interaction of light with an object of effective length scale equal to the thickness of the Ga embedded region.

The SEM image shown below reveals that the depth of the Ga nanodroplets is higher in PDMS 20. Since it has more layers of Ga nanodroplets, gap plasmon contribution from all the layers of PDMS 20 will occur at a wavelength higher than that in the case of PDMS 5. Therefore, the major spectral features of PDMS 20 are expected to be red-shifted compared to PDMS 5.

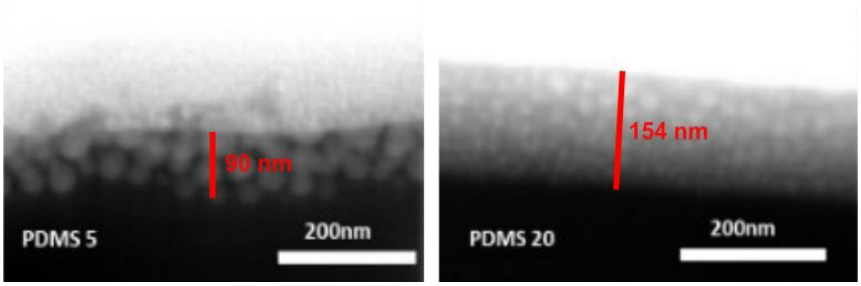

Figure 22: The depth of Ga nanodroplets in the case of PDMS 20 (more oligomer content) is more than that of PDMS 5 (less oligomer content).

3.2 Mechanoresponsive on stretching the sample (uniaxial linear stretch)

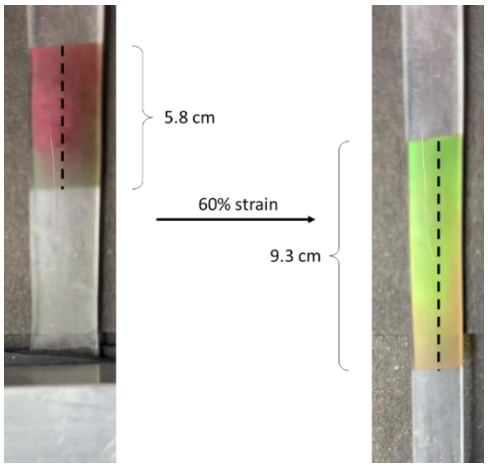

Figure 23: Change of color of Ga deposited PDMS, occurring due to a strain of 60%.

The change of color of the sample is attributed to the change in the chromogenic structure of Ga nanoparticles interacting with the incident light. For two adjacent particles in a given layer, stretching will increase the inter-droplet gap filled with PDMS oligomers with a refractive index of 1.4. Hence, the study is necessary to determine the interaction of electromagnetic fields with two Ga droplets in PDMS placed near each other with varying gaps.

3.3 Study of two droplets of the same radius in an environment of PDMS

For finite difference time domain (FDTD) simulations, the commercial software package Lumerical is used. The two spherical spheres are placed close to each other with a particular gap inside the FDTD region. Perfectly Matched Layer Boundary condition is applied on all sides. The source used is Total Field Scattered Field (TFSF), and the reflectivity monitor is placed outside the TFSF region behind the source.

In this section, we will show the following:

3.3.1 For polarisation vector along the Gap between the spheres

1) The fluidic interactions of liquid oligomers result in Ga nanodroplets of a radius of no more than 50nm. When two Ga nanospheres of the same radius (< 50nm) are embedded in PDMS (dielectric of refractive index 1.4), they exhibit gap plasmon resonance in the visible range if the polarisation vector is along the Gap between the spheres. It is the primary cause of resonance in this configuration.
2) The gap plasmon resonance blue shifts with the increase in the Gap (Figure 24a).
3) The resonances at shorter wavelengths correspond to collective dipole and Quadrupole oscillations of electrons in both spheres.
4) With the decrease in radii, the plasmon resonance blue shifts (Figure 25b).

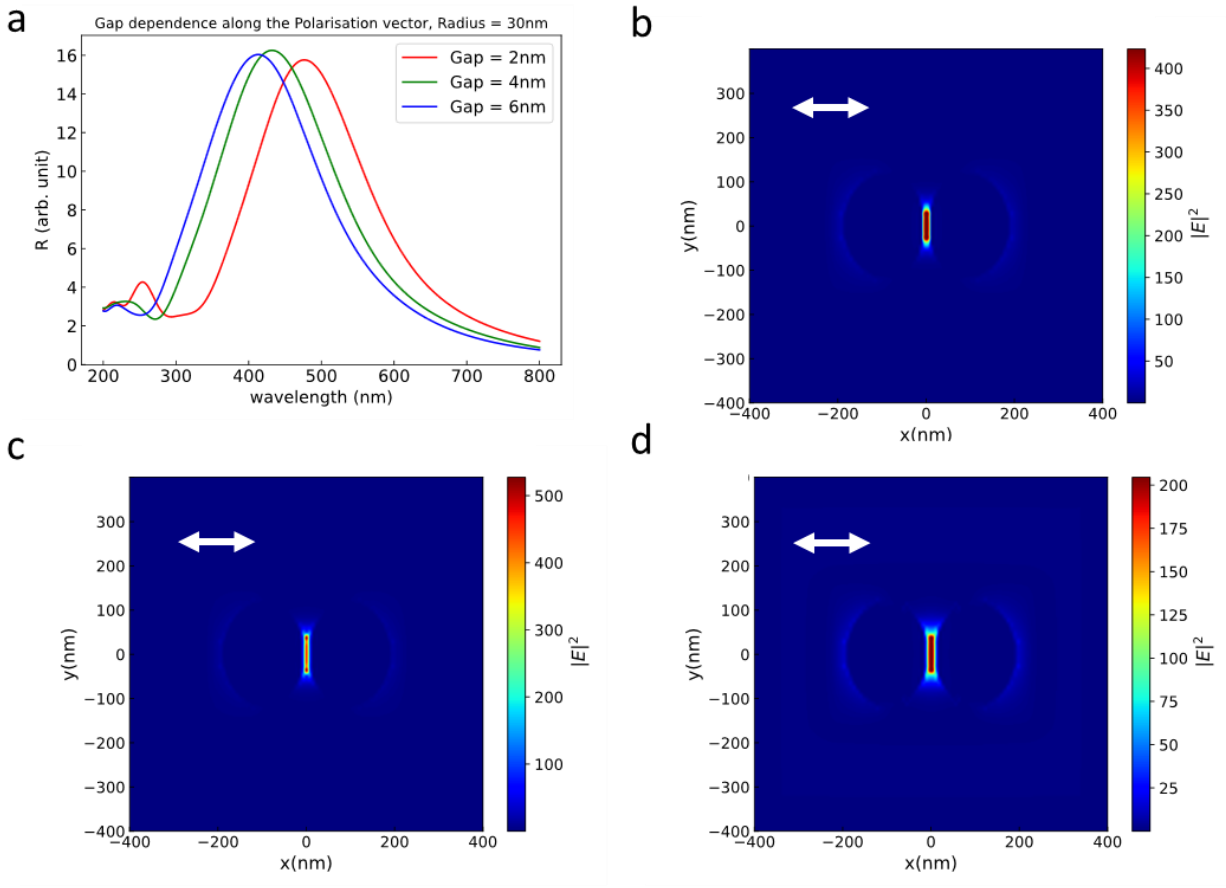

Figure 24: Gap plasmons variation with dielectric Gap. a) Reflectivity plot obtained from FDTD simulation. It indicates the blue-shift of the spectrum with the increase in the Gap between the two spheres. The Gap plasmon resonance occurs in the visible region. b-d) The field plots plotted at the gap plasmon resonance for a gap of 2, 4 and 6 nm respectively.

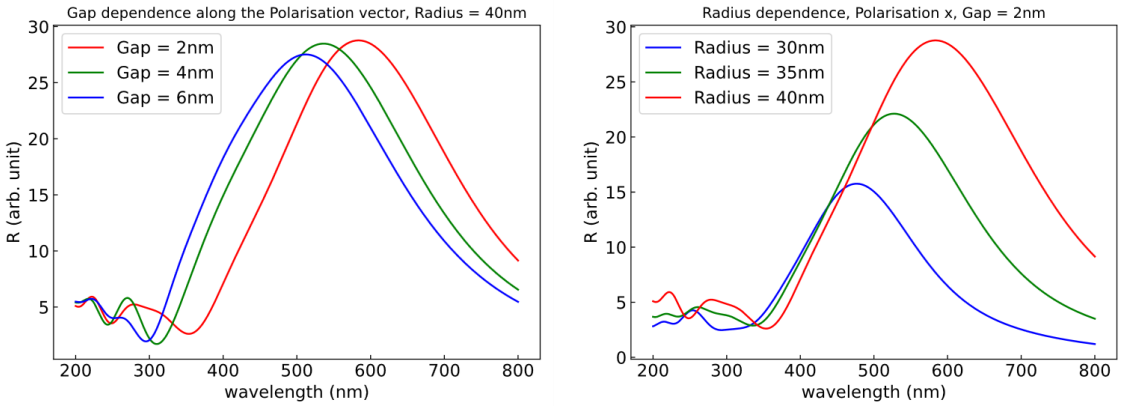

Figure 25: Reflectivity plot from two spheres at the different gap (left) and different radii(right).

3.3.2 For polarisation vector perpendicular to the gap between the spheres

1) The polarization vector perpendicular to the gap shows negligible interaction between the fields scattered by two nanospheres. This phenomenon is effectively a single-particle effect and can be approximated as two independent single-particle scattering events co-occurring, as indicated by the simulation results in Figure 26.

2) Since these scatterings are independent and the Ga droplets are spherical, we can apply Mie theory to understand the spectral features in the UV region.
3) The primary cause of resonance is the collective oscillation of electrons in the dipole mode of the spheres.
4) The reflectivity spectra of these systems of spheres are independent of the gap between them.

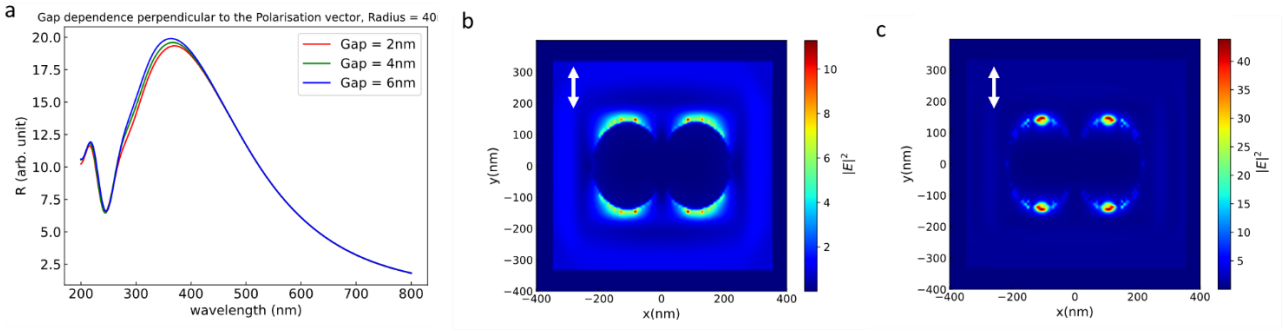

Figure 26: Independent scattering by the two nanospheres in the case where polarisation is perpendicular to the direction of the gap. a) The reflectivity spectrum does not change by increasing the gap between the spheres. The major resonance is due to dipole resonance at the UV region, as plotted in (b). The minor peak is due to quadrupole resonance at the extreme UV region, as shown in (c).

The above simulation readily predicts the following spectral behavior observed experimentally on applying a uniaxial strain to the sample. We observe that the spectral features in the UV region do not change, and those in the visible and IR region get blue-shifted (Figure 26a).

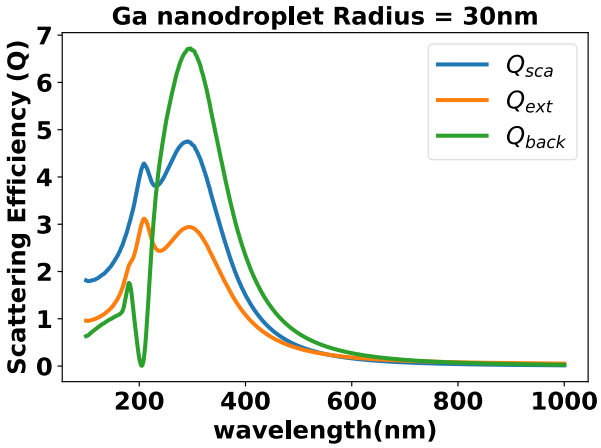

Figure 27: Efficiencies of Scattering, Extinction, and back-scattering of Ga sphere of 30 nm radius embedded in a medium of refractive index 1.4 as calculated from Mie Theory.

The UV spectral features can be attributed to the independent single-particle scattering of light by the individual Ga nanodroplets resulting from the interaction of those electric field components perpendicular to the gap between particles. As shown previously with the two-particle simulation, the spectral features due to single-particle scattering do not exhibit significant change. As shown above, in Figure 27, the scattering by the individual Ga spheres is limited to the UV region. On the other hand, the spectral features in the visible and IR region get blue-shifted, whose cause can be attributed to the increase in the inter-particle gap due to the uniaxial stretching (Figure 26a and 28).

In the following, we show the blueshift trend in the visible region and the null shift in the UV region of reflectivity spectra of different samples with respect to uniaxial stretching (Figure 28). It is corroborated by multiple and distinct simulations exhibiting the aforementioned spectral trends on applying a uniaxial strain.

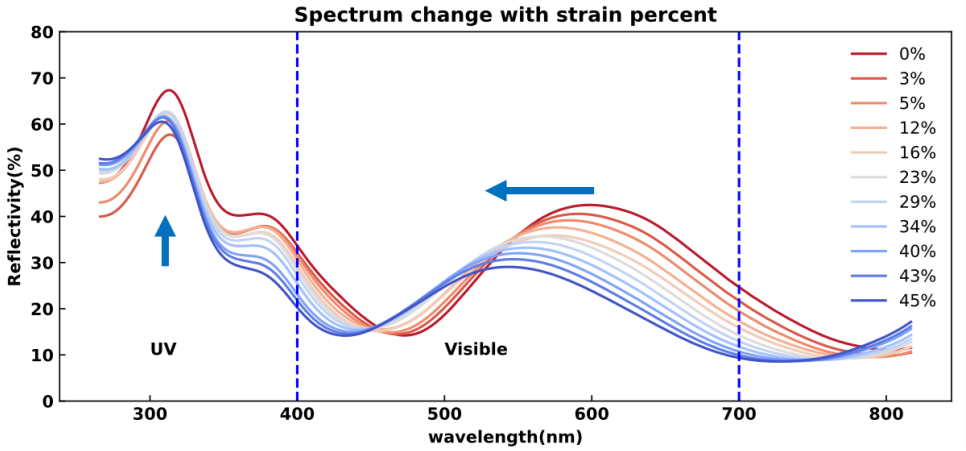

Figure 28: Experimentally obtained spectra of Ga deposited PDMS sample (Thickness: 100nm, Temperature: 35C, PDMS 10) at different strain percentages. The blue shift occurs in the visible and IR regions, whereas no such shift is observed in the UV region.

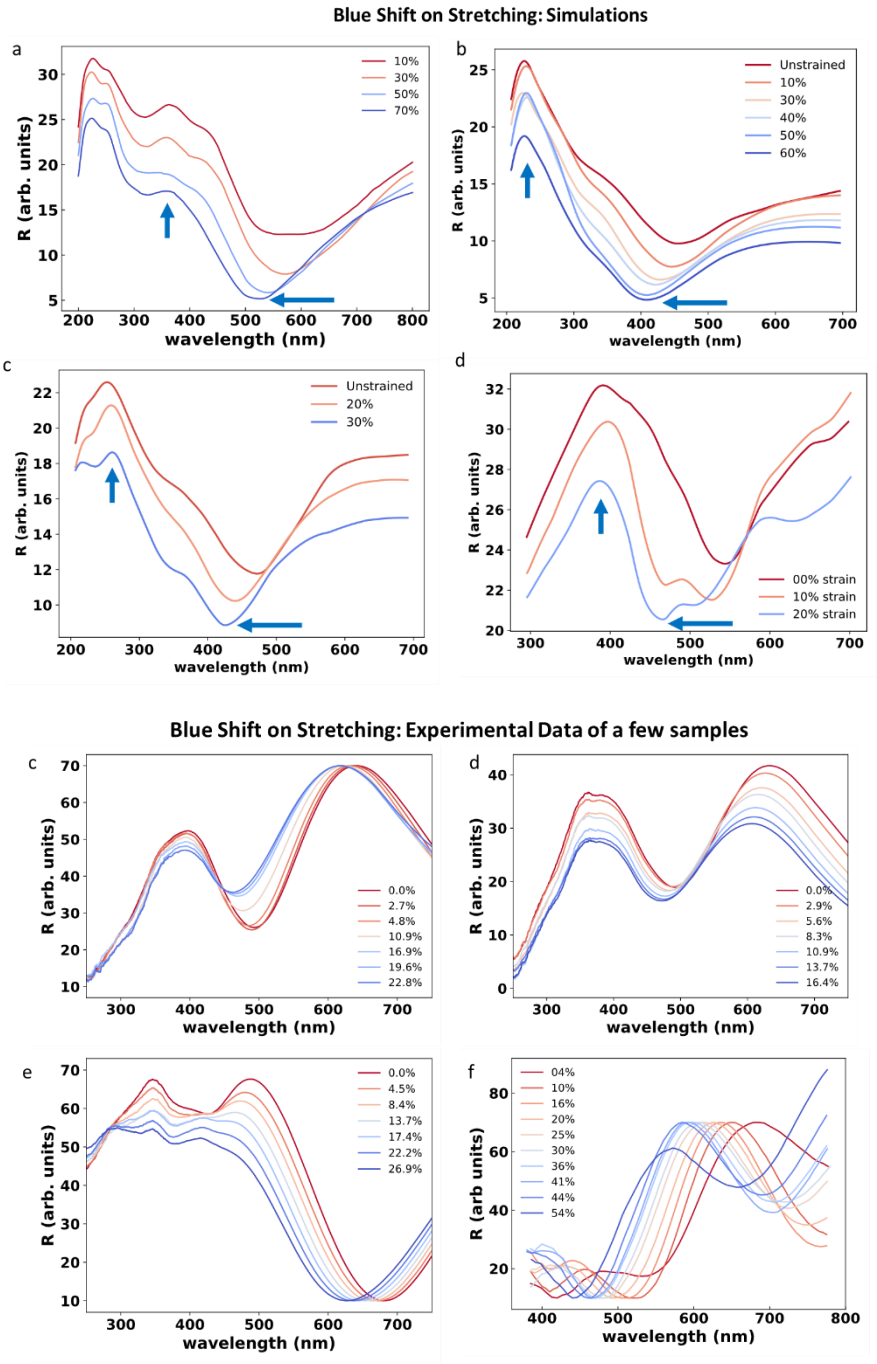

Figure 29: Blue shift in the visible region and null-shift in the UV region of simulated and experimental spectra of Ga deposited PDMS sample at different strain percentage. a, b, c, d, Reflectivity spectra obtained from four different simulated structures varying in number of layers, and size distributions. e, f, g, h, Experimentally obtained reflectivity spectra of four different fabricated samples.

4. Color characterization and other applications

4.1 CIE coordinates from Reflectivity Spectra

The following steps are followed to obtain the CIE x and y coordinates for a given reflectivity spectrum [6].

1. A reflectivity spectrum obtained in arbitrary units and normalized with a known reference (such as a silver mirror) is needed as an input.
2. We have the illuminant D65 spectrum as the source of light that determines illumination. The response of human eyes to different wavelengths is encoded in terms of three functions called the color-matching functions, denoted by $\bar{x}, \bar{y}$ and $\bar{z}$.

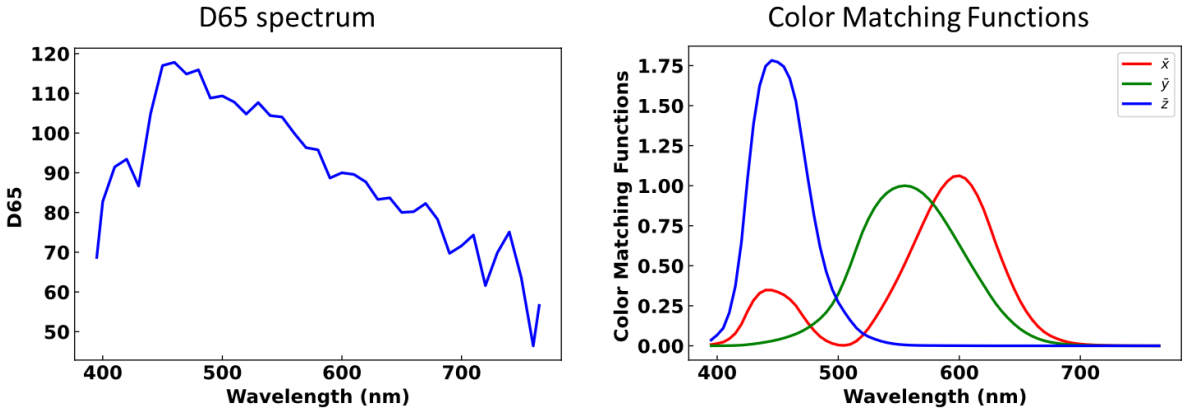

Figure 30: Data that encapsulates the illuminant and response of eyes to a spectrum. a, Spectrum of illuminant D65. b, Color matching functions.

3. The tristimulus for white light (D65) is obtained by,

$$X_{D65} = \frac{\sum \bar{x}.D65}{\sum \bar{y}.D65} = 0.950$$

$$Y_{D65} = \frac{\sum \bar{y}.D65}{\sum \bar{y}.D65} = 1.000$$

$$Z_{D65} = \frac{\sum \bar{z}.D65}{\sum \bar{y}.D65} = 1.088$$

where the dot (.) operation gives another array with each element as obtained from the elementwise multiplication of the two arrays. The expression $\sum \bar{x}.D65$ refers to the sum of the elements in the array obtained by elementwise multiplication of $\bar{x}$ and $D65$.

4. The white point is given by,

$$x_{D65} = \frac{X_{D65}}{X_{D65} + Y_{D65} + Z_{D65}} = 0.313$$

$$y_{D65} = \frac{Y_{D65}}{X_{D65} + Y_{D65} + Z_{D65}} = 0.329$$

5. Then we calculate S by elementwise multiplication of the reflectivity spectrum and $D65$,

$$S = R \cdot D65$$

6. The tristimulus values are then obtained for S,

$$X = \frac{\sum \bar{x}.S}{\sum \bar{y}.D65}$$

$$Y = \frac{\sum \bar{y}.S}{\sum \bar{y}.D65}$$

$$Z = \frac{\sum \bar{z}.S}{\sum \bar{y}.D65}$$

7. The CIE x and y coordinates can be obtained from the tristimuli values as follows,

$$x = \frac{X}{X + Y + Z}$$

$$y = \frac{Y}{X + Y + Z}$$

The CIE chromaticity coordinates are given by x and y, while the value of Y denotes the object's brightness from which the reflectivity spectrum is measured.

RGB and Hue from CIE xyY coordinates

For a given color specified by CIE x, y and Y, one can obtain the RGB values by following steps:

1. We obtain z by,

$$z = 1 - x - y$$

2. The rest of the tristimuli values are determined as,

$$X = \frac{xY}{y}$$

$$Z = \frac{zY}{y}$$

3. We obtain $R', G', and\ B'$ values from the following matrix operation,

$$\begin{pmatrix} R' \\ G' \\ B' \end{pmatrix} = \begin{pmatrix} 3.2404542 & -1.5371385 & -0.4985314 \\ -0.9692660 & 1.8760108 & 0.0415560 \\ 0.0556434 & -0.2040259 & 1.0572252 \end{pmatrix} \begin{pmatrix} X \\ Y \\ Z \end{pmatrix}$$

4. Let S′ and S belong to the corresponding values in (R', G', B') and (R, G, B) respectively.

5. The values of R, G and B are obtained by the following conditional operation

If $S' < 0.0031308$,

$$S = 12.92\, S'$$

Else,

$$S = 1.055 \quad S'^{(1.0/2.4)} - 0.055$$

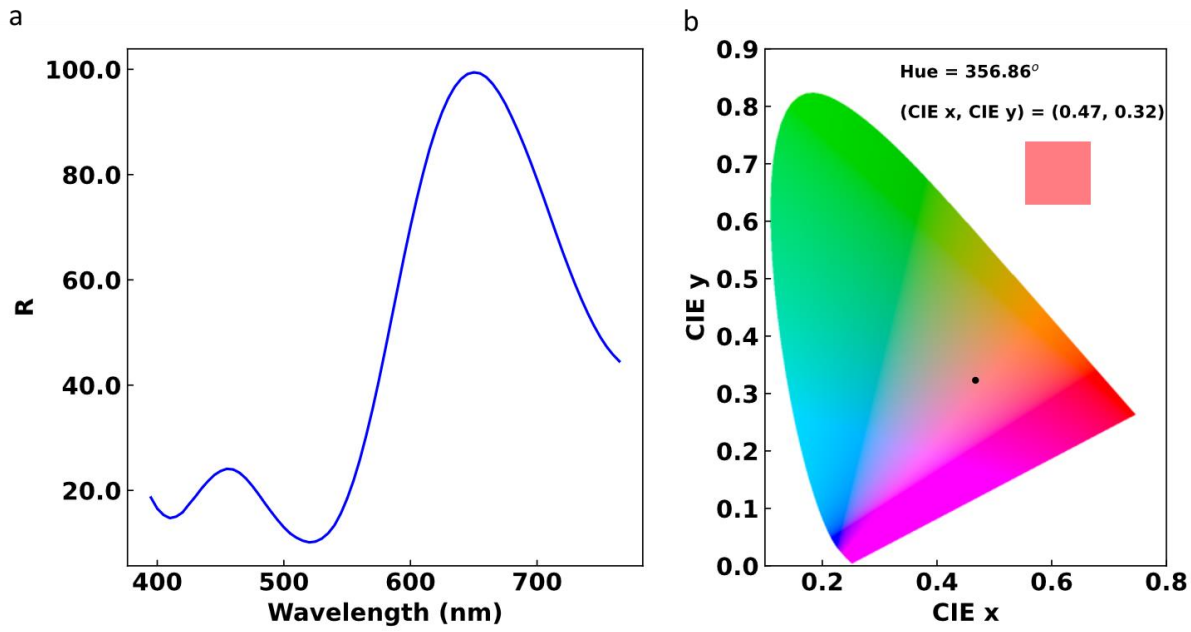

Figure 31 Reflectivity plot and corresponding color coordinates. a, Reflectivity spectrum obtained from spectrophotometer and normalized with respect to the reference. b, The CIE x and y coordinates and hue corresponding to the reflectivity spectrum.

6. Having obtained the values of R, G, B, we obtain hue by the following procedure:
   a. We evaluate C_{max}, C_{min}, and Δ as,

$$C_{max} = max(R, G, B)$$

$$C_{min} = min(R, G, B)$$

$$\Delta = C_{max} - C_{min}$$

   b. If $\Delta = 0$, the value of the hue is $H = 0$
   c. If $C_{max} = R$, the value of the hue is $H = 60 \times \left(\frac{G-B}{\Delta}\right)$
   d. If $C_{max} = G$, the value of the hue is $H = 60 \times \left(\frac{B-R}{\Delta} + 2\right)$
   e. If $C_{max} = B$, the value of the hue is $H = 60 \times \left(\frac{R-G}{\Delta} + 4\right)$
7. The hue range obtained from the above procedure is from 0 to 360 degrees. In cases where the hue values are reported more than 360 degrees in the main text, the hue is to be

wrapped to the range mentioned above by a modular division by 360. For example, hue value of 400 degrees is equivalent to 40 degrees (= 400 mod 360).

4.2 Determination of Curvature from the image.

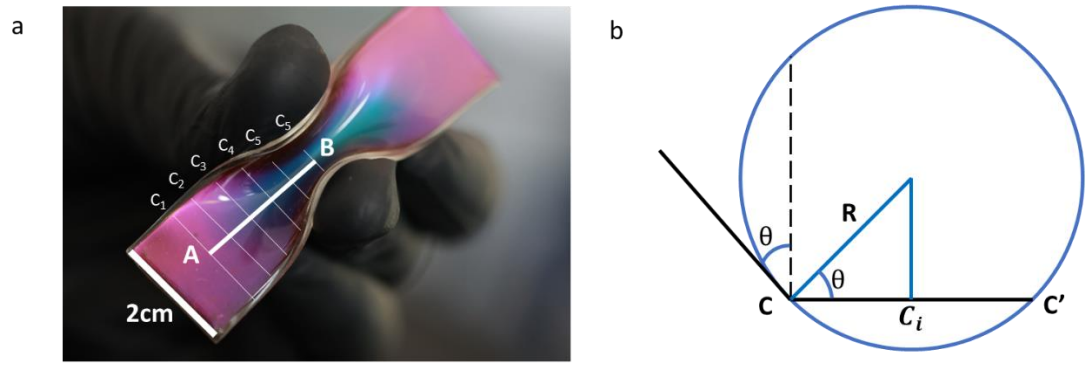

Figure 32 Determination of the radius of curvature from the image along the line AB. a, Optical image of the sample showing a color change with varying curvature. b, The geometrical construction used to determine the radius of curvature for chord length C_i.

To obtain the curvature from point A to B along the line AB we assume that linear variation of the edge angle from 0 to 90 degrees. The chord lengths C_i (= CC') are determined to vary from 2cm to 0.47 cm at intermediate intervals along AB. The geometry (Figure 32b) is used to determine the curvature using the above data.

The corresponding hue can be computed by the abovementioned method after determining the RGB values using image processing software (ImageJ FIJI).

$$R = \frac{C_i}{2\,cos\,\theta}$$

5. References

1. Style, R. W. & Dufresne, E. R. Static wetting on deformable substrates, from liquids to soft solids. *Soft Matter* **8**, (2012).
2. Ravazzoli, P. D., González, A. G., Diez, J. A. & Stone, H. A. Buoyancy and capillary effects on floating liquid lenses. *Phys Rev Fluids* **5**, (2020).
3. Smith, J. D. *et al.* Droplet mobility on lubricant-impregnated surfaces. *Soft Matter* **9**, 1772–1780 (2013).
4. Cai, Z., Skabeev, A., Morozova, S. & Pham, J. T. Fluid separation and network deformation in wetting of soft and swollen surfaces. *Commun Mater* **2**, (2021).
5. Lenham, A. P. The optical constants of gallium. *Proceedings of the Physical Society* **82**, (1963).
6. McCarley, J. E., Green, C. E. & Horowitz, K. H. Digital System for Converting Spectrophotometric Data to CIE Coordinates, Dominant Wavelength, and Excitation Purity. *J Opt Soc Am* **55**, (1965).